Accepted ms – J. Cont. Hydrology 2018 – doi 10.1016/j.jconhyd.2018.05.007

Evaluation of single- and dual-porosity models for reproducing the release of external and internal tracers from heterogeneous waste-rock piles

S. Blackmore[1,2], D. Pedretti[3,*], K.U. Mayer[1], L. Smith[1], R. D. Beckie[1]

[1] Earth, Ocean and Atmospheric Sciences, University of British Columbia (UBC), Vancouver, BC, Canada

[2] BGC Engineering Inc. 500-980 Howe St. Vancouver, BC, Canada

[3] Geological Survey of Finland (GTK), Espoo, Finland. *Corr. Author: daniele.pedretti@gtk.fi

Highlights:

- Modeling transport of internal and external tracers reveals mass transfer mechanisms in mine waste rock
- Heterogeneity determines non-Fickian scaling of tracer breakthrough curves
- Single- and dual-porosity models do not fully capture tracer release from waste rock
- Waste-rock piles are best conceptualized as multi-porosity systems

Abstract: Accurate predictions of solute release from waste-rock piles (WRPs) are paramount for decision making in mining-related environmental processes. Tracers provide information that can be used to estimate effective transport parameters and understand mechanisms controlling the hydraulic and geochemical behavior of WRPs. It is shown that internal tracers (i.e. initially present) together with external (i.e. applied) tracers provide complementary and quantitative information to identify transport mechanisms. The analysis focuses on two experimental WRPs, Piles 4 and Pile 5 at the Antamina Mine site (Peru), where both an internal chloride tracer and externally applied bromide tracer were monitored in discharge over three years. The results suggest that external tracers provide insight into transport associated with relatively fast flow regions that are activated during higher-rate recharge events. In contrast, internal tracers provide insight into mechanisms controlling solutes release from lower-permeability zones within the piles. Rate-limited diffusive processes, which can be mimicked by nonlocal mass-transfer models, affect both internal and external tracers. The sensitivity of the mass-transfer parameters to heterogeneity is higher for external tracers than for internal

tracers, as indicated by the different mean residence times characterizing the flow paths associated with each tracer. The joint use of internal and external tracers provides a more comprehensive understanding of the transport mechanisms in WRPs. In particular, the tracer tests support the notion that a multi-porosity conceptualization of WRPs is more adequate for capturing key mechanisms than a dual-porosity conceptualization.

Keywords: *waste-rock piles, acid-rock drainage, heterogeneity, tracer tests, dual porosity, mass transfer.*

1. Introduction

Accurate predictions of solute release from waste-rock piles (WRPs) are paramount for decision making in mining-related environmental processes. Such predictions rely on robust conceptual and mathematical models of transport, which are informed by experimental observations in field and laboratory environments (e.g. Amos et al., 2014; Jodeiri Shokri et al., 2016; Lahmira et al., 2017; Lefebvre et al., 2001; Lorca et al., 2016; Pedretti et al., 2015, 2017; Smith and Beckie, 2003). Tracer tests are experimental tools widely used nowadays for the identification and quantification of dominant transport mechanisms in the subsurface (e.g. Cvetkovic et al., 2016; Liang et al., 2016; Molinari et al., 2015; Wilson et al., 2016; Xie et al., 2016; Zaramella et al., 2016). In WRPs, tracer tests can be used to characterize complex unsaturated flow and transport patterns, which are controlled by physical and chemical heterogeneities (e.g. Blackmore et al., 2014; Eriksson et al., 1997; Marcoline, 2008; Neuner et al., 2013; Nichol et al., 2005; Peterson, 2014; Silva et al., 2014). Although our work mainly focuses on conservative tracer tests, reactive compounds can also be used to identify geochemical processes within the waste rock at both laboratory and field scales (e.g. Prasad and Kumar, 2015; Ramírez-Pérez et al., 2013; Strömberg and Banwart, 1999).

External tracers are used in the majority of hydrogeological applications (e.g. Molinari et al., 2015; Pedretti and Bianchi, 2018) and can be applied either at one location (e.g. an injection well) or on a surface, such as in the case of WRPs through an artificial rain event. In the context of WRPs, Blackmore et al. (2014) analyzed the results of an external tracer test performed on waste rock in laboratory columns and experimental piles in the field. The results showed that the physical heterogeneity of these materials generates non-symmetric breakthrough curves (BTCs) characterized by persistent concentrations at times longer than the time of BTC peaks, a behavior

defined in the literature as BTC tailing (e.g. Pedretti and Bianchi, 2018). Using a combination of mathematical techniques, Blackmore et al. (2014) found that a one-dimensional (1D) dual-porosity-based mobile-immobile (MIM) model was able to simulate observed BTCs, while a 1D advection-dispersion equation (ADE) solution could not reproduce BTC tailing. The MIM model is based on a 1D advection-dispersion equation (e.g., Domenico and Schwartz, 1990), which embeds a nonlocal operator to simulate the non-equilibrium storage of the tracer in an "immobile" domain and allows for fitting non-Fickian tailing on experimental BTCs (e.g. van Genuchten and Wierenga, 1976; Simunek et al., 2003).

Internal tracers are defined as those compounds that already exist in the subsurface and that are mobilized in response to external stresses, such as a natural or artificial recharge event or a change in geochemical conditions of the systems. Internal tracers offer an alternative to understand and parameterize the formation and persistence of drainage generated from in-situ geochemical processes. In WRPs, soluble by-products from chemicals used in blasting operations at mine sites are potential internal tracers present on the surface of waste-rock particles throughout the entire pile. These internal tracers are likely associated with the full spectrum of grain sizes, including the finest-grained matrix materials. Examples of these compounds commonly associated with mine sites include nitrogenous compounds (ammonia and nitrate) and perchloride (Aziz and Hatzinger, 2008; Bailey et al., 2013; Chlot et al., 2015; Jermakka et al., 2014; Karlsson and Kauppila, 2016; Mahmood et al., 2017; Revey, 1996). In other contexts, these types of tracers have been associated with blasting occurring during road construction (e.g. Degnan et al., 2016).

There is limited evidence or literature documenting the use of internal tracers to provide quantitative insights into WRP flow and transport processes. In Bailey et al. (2013), concentrations of total sodium and chloride were used as conservative tracers to identify the first flush of water through the waste rock. Bailey et al. (2013) concluded that blasting agents proved effective for quantifying, for instance, the small portion of WRPs that has been flushed compared with its total drainage system (less than 10% in their case). At present, however, we know of no attempts to interpret internal tracers using a process-based model, such as a dual-porosity model.

This study analyzes external bromide and internal chloride tracer data from two well-characterized experimental WRPs at the Antamina Mine site in Peru. Bromide and chloride BTCs were observed in the piles over 1000 days, providing a sufficiently long data record to evaluate

transport mechanisms occurring in the piles. The interpretation of the tests is carried out using a mathematical approach similar to the one adopted by Blackmore et al. (2014) and includes temporal-moments analysis and MIM-based modeling. We analyze and discuss the results, focusing on the information that each tracer is able to provide based on the resulting parameterization obtained from the fitting of the experimental curves.

Based on the results and analysis from the Antamina data set, the specific goals of this work are: (1) to present an approach to quantify transport processes occurring within WRPs using both external and internal tracers, and (2) to discuss the advantages and disadvantages of each tracer to assess specific mechanisms occurring within heterogeneous waste-rock piles. The ultimate purpose of this analysis is to evaluate whether the combined use of internal and external tracers can provide a more complete assessment of the mechanisms and processes controlling solute transport in WRPs compared to the assessment performed by the analysis of an individual tracer. In particular, the use of different tracers suggests a modeling approach able to more effectively describe transport in heterogeneous WRPs (e.g., through a multi-porosity conceptualization of the system).

2. Materials

2.1 Site description

The experimental WRPs are located at the Antamina Mine, about 270 km north of Lima (Peru) in the Peruvian Andes (Figure 1a). The mine has a typical Andean climate with two distinct seasons; a wet season from October to April and a dry season for the remainder of the year. The area receives between 1200 mm and 1500 mm of precipitation per year, of which approximately 80% falls in the wet season as rain. Over the 1000 day study period (from June 2009 to May 2012), the Antamina site received a total of 3900 mm of precipitation. Median air temperatures (T) at Antamina are around T = 5.5 ^{o}C, with limited seasonal and daily fluctuations (e.g. Lorca et al., 2016).

Waste rock produced at Antamina is subdivided into three classes named A, B and C, based on their expected reactivity and potential to generate poor-quality drainage (i.e., lower pH values and higher metal loads). Class A is expected to have the greatest potential for producing poor-quality drainage. This material represents rocks close to the highly mineralized zones of the mine with

larger amount of sulfides, lower amount of carbonates and finer grain size than Class B and C. Class C has the lowest potential to generate poor-quality drainage, representing coarse carbonate-rich rocks with low sulfide content. Class B material is described as having an intermediate potential between Class A and C. Figure 2 shows the grain size distributions (GSD) and soil-water characteristic curves (SWCC) of the two classes A and C, obtained from previous studies (e.g., Bay et al., 2009; Peterson, 2014; Speidel, 2011). Note that about 90% of the Class C material has a particle size greater than 10 mm, while Class A material has a much higher component of material finer than 1 mm (approximately 20%).

There are five experimental WRPs at Antamina, each with the same geometry of 36 m (l) × 36 m (w) × 10 m (h) (Figure 1b) and waste-rock mass (M_{WR}) of about M_{WR} =19000-25000 tonnes. This study focuses primarily on Piles 4 and 5. Pile 4 contains >80% Class C material and <20% Class B material. Pile 5 contains about 50% of Class A and 50% Class C waste rock (Figure 1d). All experimental WRPs were constructed using an end-dumping approach, resulting in a sequence of depositional units or "tipping phases" (TPs) with an angle of repose close to 37^{o}. In a cross-sectional view, all planar contact surfaces between TPs dip parallel to the external slope (or batter).

At the base of each WRP is one large 36 m (l) × 36 m (w) lysimeter, D, to collect the exfiltrating drainage. Three 4 m x 4 m sublysimeters, A, B and C (Figure 1c) are embedded within lysimeter D along the centerline of the WRP to collect drainage from specific sections of the WRPs, similar to the approach described by Nichol et al. (2005). Figure 1d presents a vertical projection showing the classes of waste rock intersected by the drainage flow paths. Because flow in WRPs is generally sub-vertical (e.g. Amos et al., 2014), sublysimeter C is expected to mainly reflect the flow starting as recharge from the pile batter, which has shorter flow paths than the center of the pile. On the contrary, the batter is expected to have the smallest influence on sublysimeter A and B and be more representative of flow occurring in the core of the pile, with average flow-path lengths comparable to the pile's vertical height (~10 m). Outflow drainage from all lysimeters is directed to an instrumentation hut for continuous recording of flow rates and volume via calibrated tipping buckets and for bi-weekly geochemical sampling. This includes measurements of concentration of total bromide and chloride, which are used as primary tracers in this study. For both compounds, the detection limit was established at 0.01 mg/l. Additional details about

the construction of all five WRPs, calibration of the instrumentation and other in-situ equipment can be found elsewhere (Bay et al., 2009; Corazao-Gallegos, 2007; Lorca et al., 2016; Peterson, 2014).

2.2 Tracer tests

External tracer tests were performed on Piles 4 and 5 using a similar approach. Bromide (Br^-), applied as a well-mixed solution of lithium bromide, was used as a conservative tracer because of its very low reactivity, relative absence in the mineral composition of the waste rock, and low natural background concentrations of 0.11 mg/l and 0.18 mg/l for Piles 4 and 5, respectively. Rainwater contains negligible bromide in this region, with concentrations near to or below 0.01 mg/l (Flury and Papritz, 1993). Bromide was applied in an artificial rainfall event to areas of ~14 m (w) × 24 m (l) located on the crowns (Figure 1c) of the experimental piles in January 2010, the middle of the first full wet season following the piles' construction. The total tracer mass (M_{ini}) applied was $M_{ini}^{Br-4} = 2.32 \times 10^4$ g for Pile 4 and $M_{ini}^{Br-5} = 2.28 \times 10^4$ g for Pile 5. The tracer solution was applied over a single 5-hour artificial rainfall event with rates q_r=124.8 mm/d and $q_r = 129.6$ mm/d for Pile 4 and Pile 5, respectively. These rates were selected in consideration of the piles' coarse-grained materials to be comparable to extreme rain events typical of the wet season at Antamina and to attempt to activate fast flow paths in the unsaturated WRPs (Shipitalo and Edwards, 1996), usually associated with macropores and characterized by low air-entry pressures.

Dissolved chloride (Cl^-) in the drainage from Piles 4 and 5 was adopted as an internal tracer. Although the origin of chloride in this system is not completely clear, it is likely a residual of the decomposition of perchlorate (ClO_4^-) or dissolution of Cl^--rich salts (e.g. ammonium or sodium salts). These compounds are typically associated to blasting agents present directly in the explosives and/or in explosion boosters, as documented in other mining sites (e.g., Bailey et al., 2013; Karlsson and Kauppila, 2016). Class A waste rock in Pile 5 is expected to contain a higher initial concentration of Cl^-, relative to Class B and C material, as it comes from highly-mineralized zones where more explosives were used to fragment rock into workable size fractions. Similar to bromide, Cl^-can be considered a conservative tracer because of its very low reactivity and the absence of chloride-bearing minerals within the waste-rock assemblages.

Unlike the external tracer, the exact initial mass of the internal tracer Cl^- is unknown. An estimate of this initial mass can be obtained from the cumulative mass recovered from long-running field-barrel experiments existing at the Antamina site. These field barrels contain the same type of material as present in the experimental piles. After about 1000 days of monitoring, the results showed almost-complete flushing of Cl^- measured at the base of the barrels, as concentrations were observed to drop and stabilize around 0.05 mg/l, which is comparable to chloride concentrations in typical rainfall (e.g. Andrews et al., 2013). Based on this information and assuming 100% recovery of Cl^- and homogeneous distribution of chloride-containing residue on the surfaces of the waste rock at the time of pile and barrel construction, an initial chloride mass M_{ini}^{Cl-4}=4.35 × 10^4 g is estimated in Pile 4 and M_{ini}^{Cl-5}=5.74 × 10^4 g in Pile 5, after proper volume-based rescaling. Further details of these calculations and information regarding the Antamina field-barrel analysis program can be found in Blackmore (2015).

3. Methods

3.1 Moment analysis

Cumulative bromide and chloride mass recovered at each lysimeter was determined as the zeroth moment of the observed BTCs and described as

$$M(t) = \int_{t=0}^{T} [C(t) - C_b]\, Q(t)\, \mathrm{d}t \qquad (1)$$

where C is the total concentration, C_b is the background concentrations of each compound, Q is the discharge rate measured at the lysimeters at a time t and T is the total experimental time. Bromide background concentrations in Pile 4 and 5 drainage were measured prior to the January 2010 tracer test.

Higher-order temporal moments were also calculated from the BTCs to estimate mean solute - residence time and effective solute dispersion within WRPs. We followed the approach by Eriksson and Destouni (1997), which incorporates a flow-corrected time (τ) to account for temporal variability in flow volumes and enables a direct comparison between different BTCs from different piles and lysimeters. In the following we provide the essential elements from the equations adopted for our study; the complete description and derivation of these equations is provided by Eriksson and Destouni (1997).

The mean solute resident time is estimated from the first temporal moment of the BTC ($\bar{\tau}$) defined as

$$\bar{\tau} = \frac{\int_0^\infty \tau\, M(\tau,z)\, \mathrm{d}\tau}{\int_0^\infty M(\tau,z)\, \mathrm{d}\tau} \quad (2)$$

where

$$\tau = \mathrm{T_F}\frac{V(t)}{V_\mathrm{T}} \quad (3)$$

in which $\mathrm{T_F}$ is the total experimental time, V is the time-dependent cumulative flow volume and V_T is the total cumulative flow volume observed during the experimental period. Note that M in (2) is expressed as a function of flow-corrected time.

The effective spreading is estimated from the second temporal moment of the BTC (σ_τ^2) defined as

$$\sigma_\tau^2 = \frac{\int_0^\infty (\tau-\bar{\tau})\, M(\tau,z)\, \mathrm{d}\tau}{\int_0^\infty M(\tau,z)\, \mathrm{d}\tau} \quad (4)$$

Since σ_τ^2 is a measure of spreading around the mean arrival time, which can be different among experiments, a normalized effective spreading can be expressed in terms of coefficient of variation (CV_τ) defined as

$$CV_\tau = \frac{\sqrt{\sigma_\tau^2}}{\bar{\tau}} \quad (5)$$

3.2 Numerical modeling

Mobile-immobile (MIM) models were fitted to the observed BTCs from the lysimeter D. The MIM model simulates the presence of mobile and immobile porosity. In the former, transport along the mobile porosity moves according to mechanistic processes described by the ADE (i.e. advection, pore-scale dispersion and diffusion). For the latter, transport does not occur, such that the immobile porosity acts as a temporary storage of solutes moving in the mobile zones. Solute exchange may occur between mobile and immobile zones, which is controlled by a kinetic, first-order, time-invariant mass rate coefficient ω. Mathematically, the MIM model can be written as

$$\frac{\partial(\theta_m C_m)}{\partial t} = \frac{\partial}{\partial z}\left(\theta_m D_m \frac{\partial C_m}{\partial z}\right) - \frac{\partial(q_z C_m)}{\partial z} - \Gamma_{\mathrm{im}} \quad (6)$$

where the suffixes "m" and "im" refer, respectively, to mobile and immobile. θ_m is the mobile porosity, C_m is the concentration in the mobile zone, $D_m = D^* + |\alpha_z| q_z$, D^* is the effective molecular diffusion, α_z is the coefficient of local dispersivity, q_z is the vertical flux in the unsaturated zone. The term Γ_{im} is a sink/source term that defines the non-equilibrium mass transfer occurring between mobile and immobile zones, and can be defined as

$$\Gamma_{\mathrm{im}} = \theta_{im} \frac{\partial C_{im}}{\partial t} = \omega(C_m - C_{im}) \quad (7)$$

where θ_{im} is the porosity characterizing the immobile zone, and C_{im} is the concentration in the immobile zone. The MIM model reduces to the ADE solution setting $\Gamma_{\mathrm{im}} = 0$ in (6), for instance when kinetic mass transfer does not occur and transport is restricted exclusively to the mobile porosity. We use HYDRUS-1D (Simunek et al., 2005) to solve both the ADE and MIM models. The atmospheric input parameters, the approach to estimate recharge and definition of model's boundary conditions can be found in Blackmore et al. (2014), and apply identically to Pile 4 and Pile 5 (as both WRPs are adjacent to each other at the Antamina site). Using the estimated recharge to each pile, calibrated flow parameters were found using a manual trial-and-error approach, by first matching the observed flow results for the piles (Supplementary Material) and then fitting the observed BTCs (figures presented hereafter). The resulting best-fitted parameters are reported in Table 1.

4. Analysis and Discussion

4.1 Cumulative mass recovery and temporal moments

We first analyze cumulative bromide and chloride recovery curves from the different lysimeters to gain initial insights about the behavior of internal and external tracers at different locations of the pile and time. The results are presented in Figure 3, in which the horizontal axes represent cumulative outflows normalized to the area A of each lysimeter ($Q' = \sum Q/A$). For the external tracer, the initial time (t_0) is the time of bromide application whereas for the internal tracer t_0 is the time of pile construction and waste rock deposition when chloride was present following

blasting. In the vertical axes, different normalization methods are adopted to display the mass recovery for the internal and external tracers.

For the external tracer bromide, a normalization factor (M_0) is adopted to compare the recovered mass across all lysimeters (Figure 3a,b). The factor M_0 rescales the amount of mass applied to the pile at the beginning of the bromide tracer test (M_{ini}^{Br-4} and M_{ini}^{Br-5}, respectively in Pile 4 and Pile 5) in light of the different footprints of the lysimeters. We first recall the expected dominant sub-vertical flow patterns in the piles, a postulation supported by the negligible bromide mass recovered at sublysimeter C, which is not located below the pile crown. Assuming perfectly vertical flow, M_0 can be computed as the mass of bromide applied in the area on the crown of the pile directly above each lysimeter. We thus set $M_0^{Br-4} = 0.05\, M_{ini}^{Br-4}$ and $M_0^{Br-5} = 0.05\, M_{ini}^{Br-5}$ for sublysimeters A and B, given that each of the sublysimeters represent 5% of the crown area and therefore under the assumption of vertical flow would recover 5% of the mass applied on the crown. For lysimeter D, $M_0^{Br-4} = 0.90\, M_{ini}^{Br-4}$ and $M_0^{Br-5} = 0.90\, M_{ini}^{Br-5}$, given that all bromide mass not entering sublysimeters A and B can be potentially collected by the basal lysimeter. As indicated above, no significant Br^- mass was recovered in sublysimeter C.

For the internal tracer chloride, a normalization factor is found on the basis of the total mass estimated using the field barrels (M_0^{Cl-4} and M_0^{Cl-5}, respectively in Pile 4 and Pile 5) (Figure 3 c,d). Assuming vertical flow and homogeneous distribution of Cl^- in the system, the relative Cl^- mass that could be potentially recovered by each lysimeter is proportional to the mass of chloride contained in the pile's sub-volume above each lysimeter. Note that, differently from bromide, Cl^- can exfiltrate from the entire waste-rock pile (and not exclusively from the volume below the crown). By accounting for the contribution of the batters to the normalization factors, we found that the vertical projection above sublysimeters A and B accounts for about 2% of the entire volume of the experimental piles, and above the sublysimeter C for about 1%. Thus, we set $M_0^{Cl-4} = 0.02\, M_{ini}^{Cl-4}$ and $M_0^{Cl-5} = 0.02\, M_{ini}^{Cl-5}$ for sublysimeters A and B, and $M_0^{Cl-4} = 0.01\, M_{ini}^{Cl-4}$ and $M_0^{Cl-5} = 0.01\, M_{ini}^{Cl-5}$ for sublysimeter C. For lysimeter D, $M_0^{Cl-4} = 0.95\, M_{ini}^{Cl-4}$ and $M_0^{Cl-5} = 0.95\, M_{ini}^{Cl-5}$, given that all chloride mass not entering sublysimeters A, B and C can be potentially collected by the basal lysimeter.

An initial visual inspection of the recovery curve shapes in Figure 3 indicates a different behavior for external and internal tracers in the piles. In both piles, bromide recovery curves (Figure 3 a,b) appear steeper and solute arrival times spread over a narrower time window relative to chloride curves. This observation suggests the generally faster breakthrough of external tracers relative to internal tracers. The early-time recovery from lysimeter D shows the first 50% of the total applied bromide was recovered at $Q' \approx 0.25$ in Pile 4 and $Q' \approx 0.35$ Pile 5. The total bromide recovery at the end of the observation period was about 60% to 70% in both piles. The larger than 100% mass apparently recovered from sublysimeter A in both piles, however, suggests that heterogeneity could have focused more mass towards the center of the pile than it would be expected by a homogeneous distribution of vertically oriented solute path-lines. Indeed, recovering more Br^- mass than $M_0^{Br-4} = 0.05\ M_{ini}^{Br-4}$ and $M_0^{Br-5} = 0.05\ M_{ini}^{Br-5}$, for each pile respectively, means that part of the tracer has to arrive from other places than vertically above the lysimeter, thus reflecting heterogeneity. Strong flow heterogeneity is likely occurring in WRPs (e.g. Eriksson et al., 1997; Lahmira et al., 2016, 2017; Lorca et al., 2016; Pedretti et al., 2017), and solute discharge is not expected to be equally distributed at the base of the piles. This behavior is consistent, for instance, with the experimental observations by Nichol et al. (2005) from external tracer tests.

The impact of heterogeneity on solute release from the experimental piles is also well visible from the analysis of the internal tracers (Figure 3 c,d). A first observation is that in Pile 4 the Cl^- recovered curves are quite comparable, while in Pile 5 a clear distinction is observed between Lysimeter D and the other curves. The behavior of lysimeter D curves reveal that proportionally more Cl mass is recovered in Pile 5 than in Pile 4, consistent with the expected higher amount of blasting residuals in Class A materials, which are found in larger proportions in Pile 5 than in Pile 4. However, note that the amount of recovered mass at the end of the experiment is lower than 20-25% at the end of the experimental time. It is indeed possible that field barrels (which contain materials with a more limited average particle diameters and more homogeneous grain- size distributions than experimental piles) could be more easily flushed than field-scale experimental piles (which contain materials with wider range grain- size distribution, including metric-scale boulders). The larger sampling of physical heterogeneity by experimental WRPs implies more flow channeling and, in turn, a larger part of the WRPs would have been less efficiently rinsed than under homogeneous conditions. Thus, field-scale WRPs may have received lower effluent

concentrations of chloride relative to field barrels over the same time of flushing. This phenomenon is also discussed, for instance, in Eriksson and Destouni (1997).

The recovery curves for both tracers display strong tailing, suggesting that the release of contaminants from the piles may occur at very slow rates. The observed BTCs (with concentrations above background limits) in Figure 4 suggest that the tracers are still present in the system at the end of the analyzed period. This inefficient flushing is associated with physical and mineralogical heterogeneity and the corresponding well-known scaling issues existing in WRPs linked to flow/transport channeling (e.g. Eriksson et al., 1997; Pedretti et al 2017). Quantitative evidence of the impact of flow channeling on experimental piles can be inferred from the analysis of temporal moments. Calculated first and second temporal moments for Pile 4 and 5, derived from bromide BTCs, show that the Pile 4 mean residence times ($\bar{\tau}$) are about 2× shorter and normalized spreading (CV_τ) about 4× larger relative to those values estimated for Pile 5. Specifically, mean residence times and normalized spreading from sublysimeter A and B of Pile 4 are $\bar{\tau}$ ≈140 d and CV_τ ≈0.74, whereas the same values for Pile 5 are approximately $\bar{\tau}$ ≈280 d and CV_τ ≈0.22. Temporal moment analysis for chloride assumed this tracer was pervasive on waste-rock surfaces and the likelihood of chloride existing on waste-rock surfaces within the mobile or immobile domains is equal. Calculated chloride temporal moment values indicate the mean residence times are generally comparable between Pile 4 and 5 (i.e., $\bar{\tau}$ =449 ±35 days), however normalized spreading values are quite comparable in Pile 4 (i.e., CV_τ = 0.40–0.56) and in Pile 5 (i.e., CV =0.52–0.67), contrasting with the much sharper spreading discrepancy between the piles than was observed for bromide.

For the external tracer, the shorter residence times and larger normalized spreading in Pile 4, compared to Pile 5, supports the idea of advective transport in Pile 4 being dominated by fast flow paths. Pile 4 has more coarse-grained Class C rock than Pile 5, which results in a higher effective hydraulic conductivity in Pile 4 than in Pile 5. It is noticeable that, despite Pile 4 being characterized by fast-flow transport, the effective bromide spreading is larger in Pile 4 than in Pile 5, and larger for bromide than for chloride in Pile 5. Here, effective (macro) dispersion is controlled by the strong variability in the hydraulic conductivity field (Malmström et al., 2004), thus generating more dispersion in the arrival time of solute at the base of the piles. Again, this is consistent with the channeling of flow and solutes in WRPs.

4.2 Numerical modeling

The internal and external tracers show distinctly different transport properties, even though both are conservative and transported through the same waste-rock material. We hypothesize that the external tracer and internal tracer access distinct flow paths and examine this hypothesis via numerical modeling. We first recall the work by Blackmore et al. (2014), who used the MIM model to fit the observed bromide BTC from Lysimeter B in Pile 5 (hereafter referred to as Pile 5B). This was done to estimate transport properties of Class A materials at the experimental-pile scale. Indeed, under the assumption of vertical flow, the BTC from Pile 5B should reflect the composition of drainage being transported through the Class A material, which constitutes the majority of waste rock situated vertically above the sublysimeter.

Here, we first extend the results by Blackmore et al. (2014) by fitting the MIM model to the Pile 5B internal tracer (Cl^-) BTC and comparing them with the corresponding ADE curves for both internal and external tracers. The ADE curves are obtained setting Γ_{im}=0 in (6) and leaving the other MIM-estimated parameters unchanged. Then, using a similar conceptual model and modeling approach targeting one specific class of materials under the assumption of vertical flow (justified by the results presented in Section 3.1), we explored transport properties of Class C, the other end-member of the waste rock, which dominates Pile 4. Since Class C is the most abundant in the vertical projection above sublysimeter A (Figure 1d) in Pile 4 (hereafter referred to as Pile 4A), it was used to analyze the external and internal tracer BTCs.

We observed that the measured bromide BTC for the external tracer in Pile 4A (Figure 4) shows a steep early arrival of contaminants and non-symmetric tails with concentrations fluctuating around C=1 mg/l. This behavior, characteristic of a dual-porosity-like solute transport, can be well fitted by a MIM model. Plotting concentrations on log scales to emphasize the behavior on the tails, we note that the curves obtained from the MIM model (Figure 4) are able to better capture the observed BTC tailing of the external tracer than the ADE model. As well, the ADE model strongly underestimates bromide concentrations at t >600 d, while the MIM sustains concentrations over longer time scales. Similarly, in Pile 5B, observed bromide BTCs shows some tailing, which is adequately simulated by the MIM model. It is noted, however, that the observed Pile 5B BTC is more symmetric than in Pile 4A, and the ADE model provides a good fit for t <600d. However, the ADE model does not sustain concentrations at longer time scales.

Fitted chloride BTCs suggest that the MIM model is able to capture the observed chloride transport processes in Pile 4A over the entire observed period, which present a slow increase in concentrations at t <200d and BTC tailing - lower concentrations later. In contrast, the ADE model largely underestimates the observed concentrations and particularly so late in the test. Similar observations can be made for Pile 5B. Both ADE and MIM models mimic the observed BTC at early stages (t <200 d); however, the ADE drops suddenly towards very low concentration at $t >$ 300d whereas the MIM model is able to simulate the average behavior of chloride BTC.

4.3 Discussion

Our results suggest that the 1D ADE model does not adequately fit the experimental results at long time scales. While this is a well-known limitation of an upscaled ADE which relies upon macrodispersion (e.g. Harvey and Gorelick, 2000; Molinari et al., 2015), we found it to be true for both types of tracers and for both piles.

The ability of the MIM model to better fit the observed curves in both piles can be attributed to the model formulation, which better represents the transport occurring as in bimodal domains (e.g. Pedretti et al., 2016; Salamon et al., 2007; Zheng et al., 2011). In the MIM, advection dominates the mobile porosity, which is where flow tends to be channeled and solute transport focused. The other porosity is not affected by flow channeling and remains immobile, such that solute can be exchanged by diffusion-like processes only. In a WRP, immobile zones can occur (for instance) as “shadow” zones below large boulders. MIM models outperform ADE models particularly at “late times”, or on the BTC tails.

In analyzing the resulting fitted parameters (Table 1) and the mass-transfer rates, ω, we note that bromide ω values for Pile 5 are more than one order of magnitude smaller than those estimated for Pile 4. However, for chloride, the resulting ω rates are comparable between the two piles. To corroborate the validity of the estimated mass-transfer rates, Figure 5 presents the results of a sensitivity analysis for this parameter. The results indicate a change of one order of magnitude in mass-transfer rates has a stronger effect on the external tracers than on the internal tracers. For the internal tracer in Pile 4A, the BTCs are relatively insensitive to the mass-transfer rate and it is therefore difficult to evaluate which mass transfer rate best fit the chloride BTC. In Pile 5B, the

model is insensitive to a $10\times$ higher mass-transfer rate (green lines), whereas the application of a $10\times$ lower value (black dotted lines) slightly underestimates observed results.

The higher estimated ω in Pile 4 than in Pile 5 for the external tracer can be attributed to a lower residence time of water in the mobile zone in Pile 4 than in Pile 5. Considering that tailing in both BTCs takes place at comparable time scales ($t \approx$600d), the mass transfer needs to be quicker in Pile 4 to generate a similar effect of transport than in Pile 5. The similar rates for chloride suggest that the relative influence of the different residence times for the piles does not affect the mass transfer process of internal tracers as much as it does the external tracer. The residence times depends on the type of tracer and the specific hydraulic properties of the pile. First, the recharge rates depend not only to the rainfall rates but also to the characteristic hydraulic properties of each pile (resulting in different VG parameters, for instance – Table 1). Second, the application of the external tracer on the crest of the pile simulates an artificial extreme rainfall event, which activates preferential flow channels, leading to a relatively short residence time. Consequently, the external tracers target flow paths that are not easily accessible by the internal tracer. Instead, internal tracers are mobilized principally by natural recharge, which is generally lower than the extreme artificial rainfall events used for the external tracer application. It is thus possible that, although there are the different grain-size distributions and spatial distribution of heterogeneity in Pile 4 and Pile 5, the mean residence time controlling mass-transfer processes of internal tracers can be very similar in the two piles and controlled by the natural rainfall events.

The different behavior of the tracers is due to the characteristics of the piles, which cannot be fully captured with the MIM model. This demonstrates the potential limitation of a dual-porosity approach to fully conceptualize transport in WRPs, which is made up of multiple porosities with different flow regimes. The MIM model assumes that the fastest portion of the flow systems acts as a unique mobile zone, all the remaining parts of the domain acting effectively as a unique immobile porosity. In reality, flow does not exclusively occur in one specific zone in WRPs. For instance, in Pile 4, the MIM model assumes that the mobile porosity is primarily represented by flow channeling through the coarser-grained materials of the pile grain-size distribution (Figure 2), and thereby generating fast arrival of bromide, resulting in heavily tailed bromide BTCs. The remaining part of the system is expected to be characterized by relatively slower matrix flow, with non-zero advective rates. The actual portion of the pile in which flow rates are zero may only

be a subset of the total porosity. However, the MIM model assumes both slow matrix and actual immobile zones to be a unique no flow zone.

Considering the behavior of internal and external tracers and given these results, we believe that a better-suited parameterization of the WRPs accounts for at least three porosities:

1. A porosity component associated with *fast flow channels*, either open voids or coarse granular materials, activated under strong recharge events, such as the one explored by the initial behavior of bromide;
2. A porosity component associated with a *slower flow in the matrix*, activated or controlled by natural rainfall events; and,
3. A *no-flow porosity* component, i.e. the immobile domain, in which transport occurs through diffusive processes only.

A three-porosity approach to transport in porous media was proposed by Zinn and Harvey (2003) and Molinari et al. (2015), which explained why effective porosities do not necessarily sum to the total porosity of a system. A three-porosity approach is embedded for instance in dual-permeability model formulations (e.g. Simunek et al., 2003). It could also be possible to account for a continuum of porosities and corresponding mass transfer rates, as in the multi-rate mass transfer models (e.g. Haggerty and Gorelick, 1995), an option not yet implemented in public releases of the HYDRUS environment and not tested here. Although a higher number of parameters could allow for a better fitting of the simulated and measured data, it may make finding a physical justification for a multi-porosity model increasingly difficult and requiring more attention when using greater than three porosities. The development of a three- or more (i.e., multi-porosity) and multi-rate modeling approach remains open for future developments.

Conclusion

Externally applied tracers and internally applied tracers are sensitive to distinct components of WRPs, and can be analyzed to characterize transport processes in heterogeneous waste-rock piles. While externally applied tracer tests require the purchase of the tracer and greater efforts to be conducted (e.g. the simulation of an artificial rainfall event and the tracer mass), internal tracers offer the advantage of being distributed throughout the waste-rock pile. At the same time, the

estimation of the existing mass of internal tracers can be difficult compared to the exact knowledge of the mass applied in external tracer tests.

In this work, we studied internal and external tracers to improve the understanding of transport processes, and to better characterize the mechanisms controlling transport. To this end, this study focused on two well-characterized experimental WRPs (Pile 4 and Pile 5) from the Antamina Mine. In both piles, a conservative external tracer (bromide) was applied to the pile's crown in an artificial high-rate recharge event. A conservative internal tracer (chloride) was present throughout the waste rock at time of placement.

The results suggest that combining internal and external tracers provides an improved understanding of processes occurring within heterogeneous WRPs compared to the analysis of individual tracers. In particular, it was observed that physical heterogeneity does not equally affect internal and external tracers. The externally applied tracer provides insight to transport along fast-flow paths, while the internal tracer is more able to identify characteristics of matrix flow. More specifically relative to this case study, the external tracer in the coarser-grained Pile 4 was substantially more sensitive to flow channeling than in the finer-grained Pile 5. In contrast, the internal tracers, more sensitive the matrix material, behaved similarly in both WRPs, with comparable BTCs shapes, moments and effective transport parameters.

The comparison of multiple tracers provides insight into a more effective parameterization of solute transport modeling in heterogeneous WRPs, relative to an analysis based of a single tracer. In particular, the tracer results suggest a conceptual model for transport in WRPs that would consist of at least three porosity components:

(1) a porosity associated with fast-flow channels, activated under strong recharge events;
(2) a porosity associated with a slower-flow matrix material, activated or controlled by natural rainfall events;
(3) a no-flow porosity, i.e. the immobile domain, in which transport occurs through diffusive processes only.

It is also possible that a continuum of porosities would allow for a better fitting of the BTCs, leading however to a more complex interpretation of the physical processes occurring in the

WRPs. The development of a three- or multi-porosity modeling approach is left open for future developments or further studies.

Acknowledgments

The authors acknowledge the comments and suggestions by two anonymous Reviewers, who have contributed to increase the quality of this manuscript.

Figures

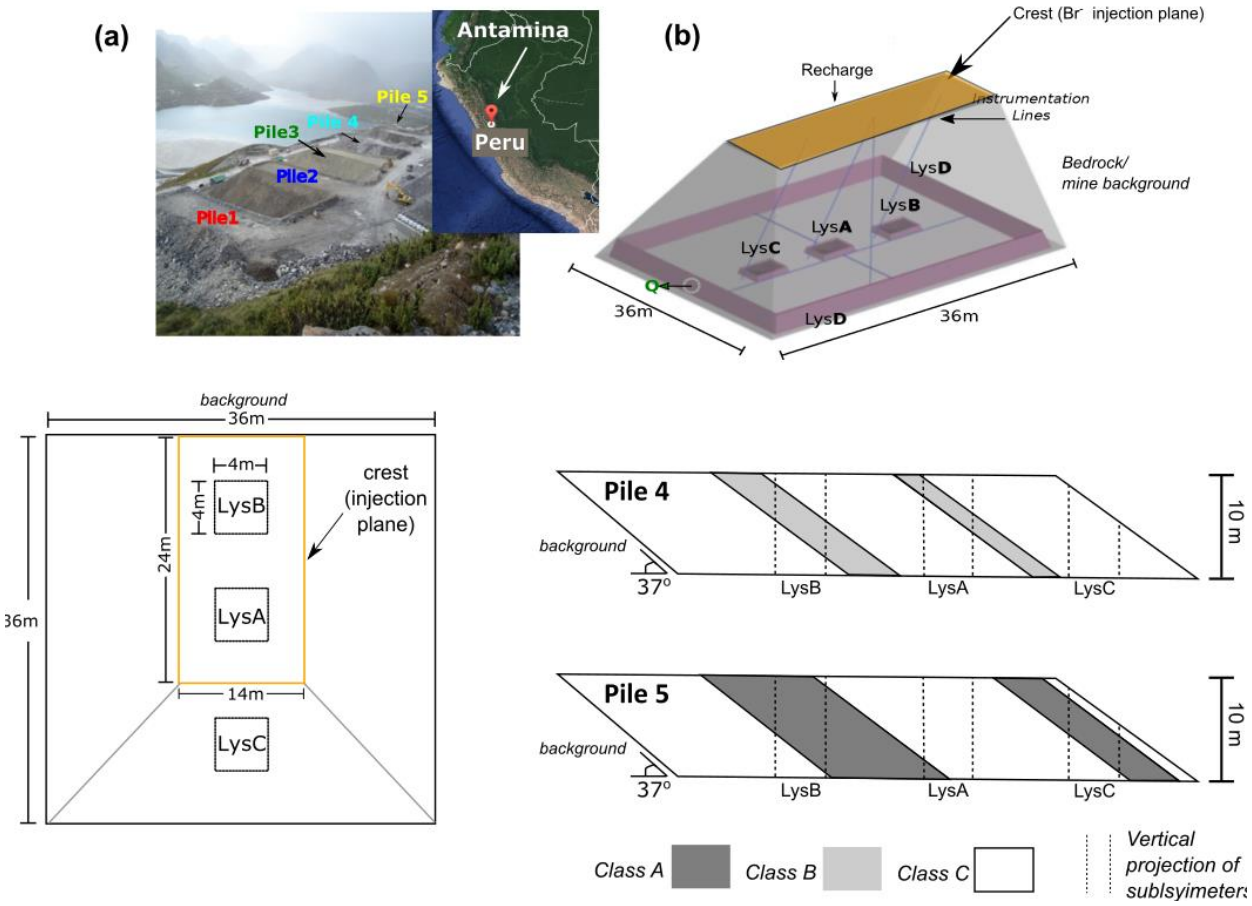

Figure 1 (a) aerial view of the Antamina experimental waste rock piles and geographical location of the site; (b) 3D conceptual model (Q=outflow); (c) schematic planar view of the piles; (d) vertical section of the piles, highlighting the geometrical distribution of waste rocks (by classes) compared with the vertical projection of the sublysimeters.

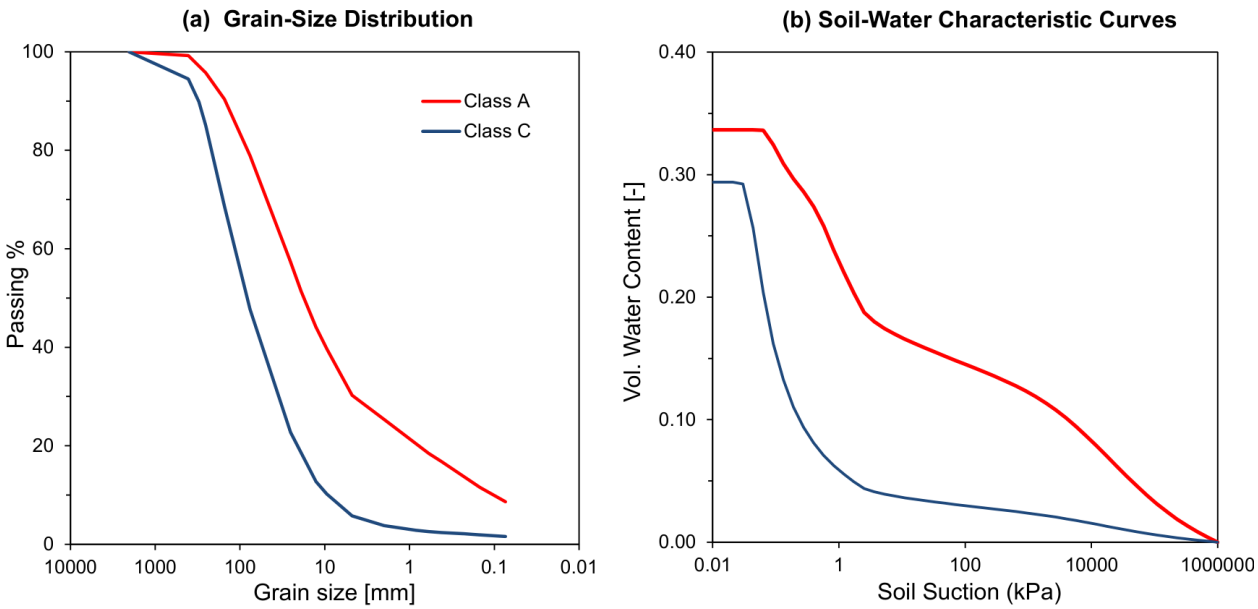

Figure 2 (a) Grain Size Distribution (GSD) and Soil-Water Characteristic Curves (SWCCs) for the two classes of waste rocks analyzed in this work.

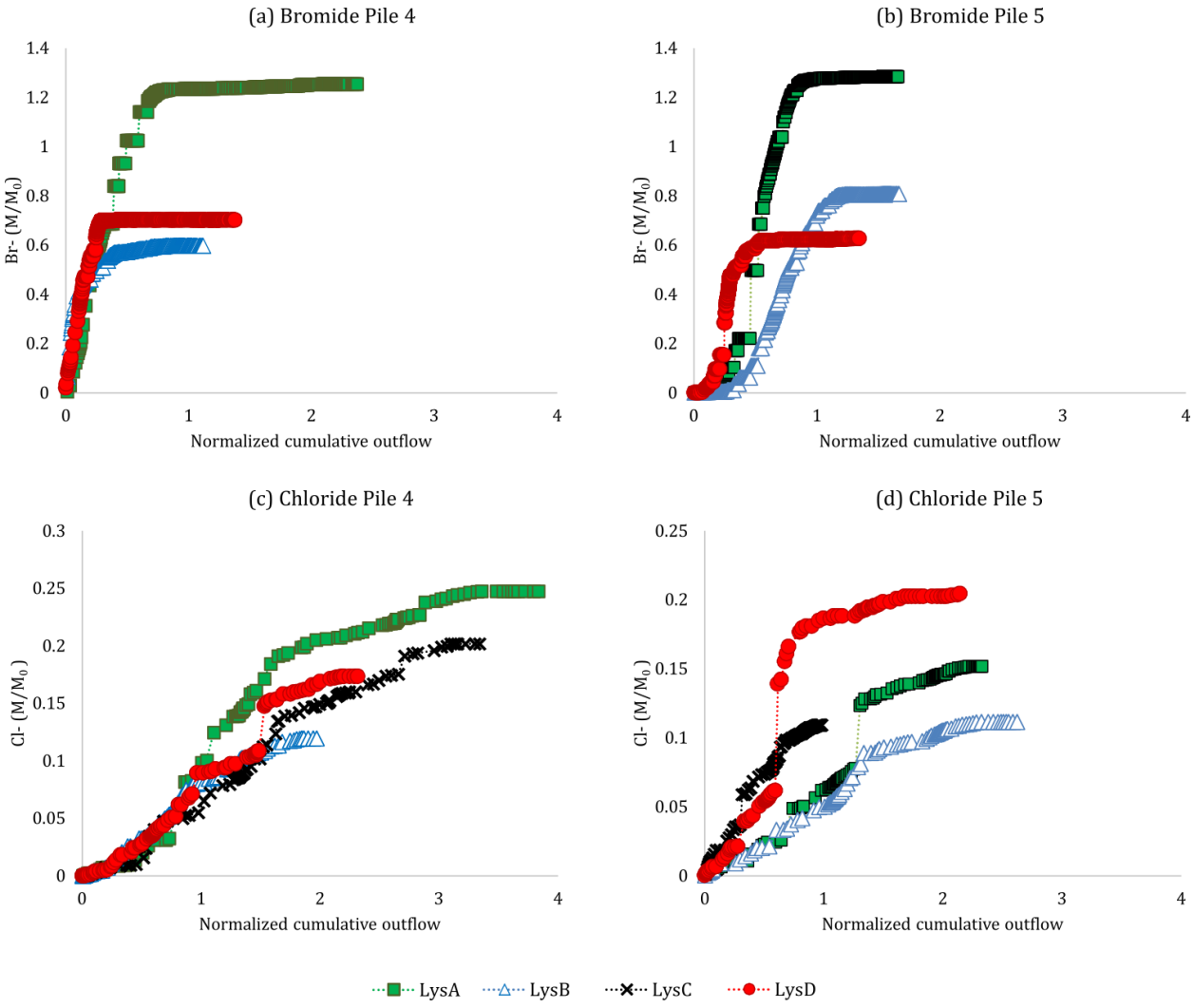

Figure 3 Cumulative mass recovery curves against normalized cumulative outflow in the four lysimeters in Pile 4 and Pile 5, respectively on the left and on the right. (a,b) Recovery curves of external tracer (bromide) normalized by the injected mass on the crown. (c,d) Recovery curves of internal tracer (chloride) normalized by the relative initial mass estimated using field barrels. The mass is proportional to the characteristic areal footprint of each lysimeter.

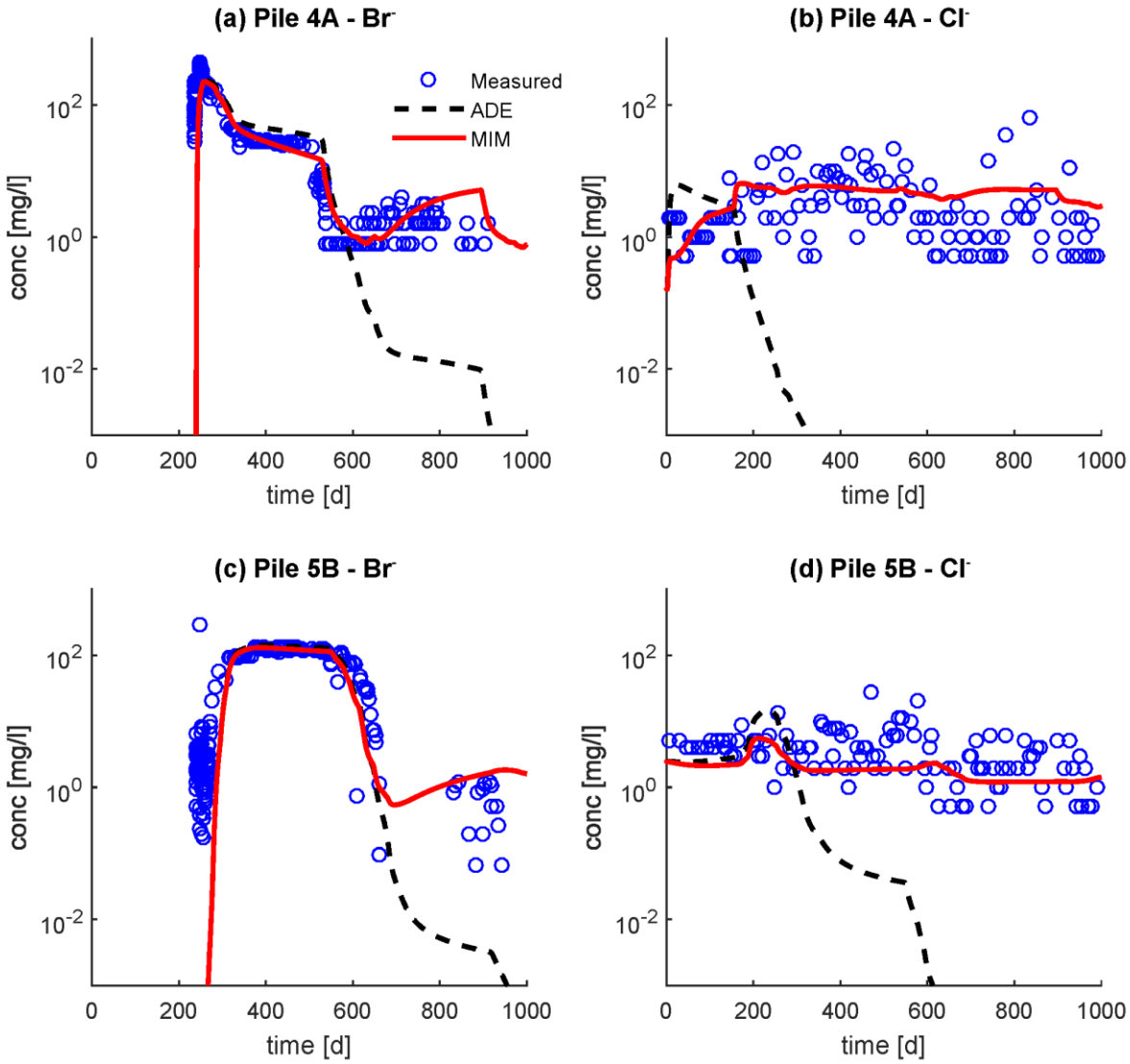

Figure 4 Experimental BTCs from external and internal tracer tests in Pile 4 – Lysimeter A and Pile 5 – Lysimeter B. The use of the vertical log scales aim to emphasize the ability of MIM models to reproduce the BTC tailing, while ADE model underestimates the observations at late time.

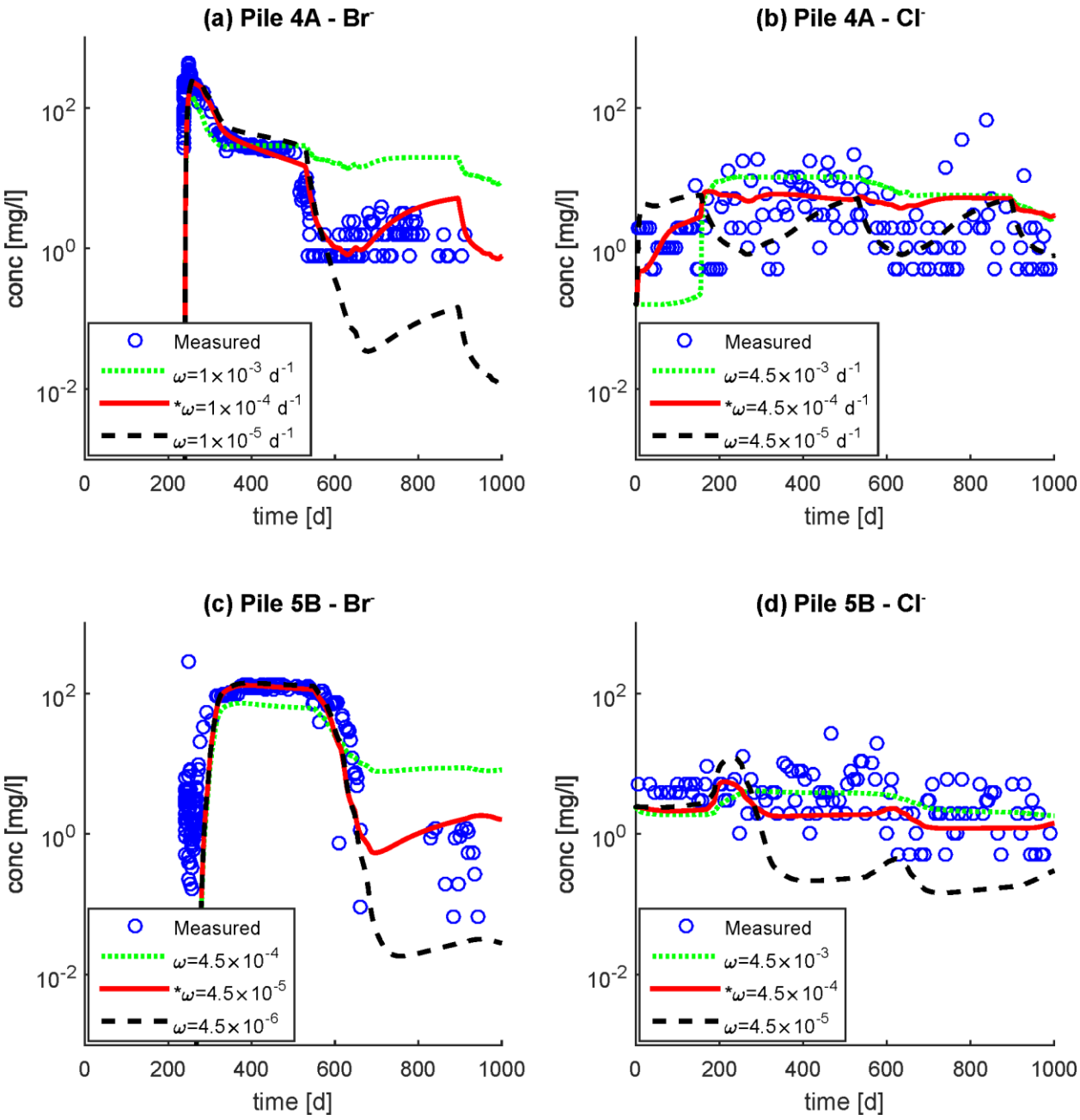

Figure 5 Sensitivity to the mass transfer rate ω in Pile 4 and Pile 5 for internal and external tracers. For each panel, the reference curve is shown in red and marked by *. The sensitivity is performed by changing ω by factors $0.1\times$ (black dotted lines) and $10\times$ (green lines).

Tables

Table 1 Calibrated parameters of flow and transport in Pile 4 and Pile 5.

Property	Units	Pile 4A	Pile 5B – top 8m	Pile 5B – bottom 2m
Waste rock class		90% C -10% B	A	C
Van Genuchten α	[m^{-1}]	2.8	1.8	5.9
Van Genuchten n	[-]	1.22	1.3	1.5
K_s	[md^{-1}]	4.0	0.06	8.0
θ_s	[-]	0.23	0.24	0.29
θ_r	[-]	0.05	0.15	0.06
θ_m	[-]	0.07	0.06	0.28
θ_{im}	[-]	0.16	0.18	0.05
λ	[m]	2.0	0.3	0.1
ω (Br^-)	[d^{-1}]	1.0×10^{-4}	4.5×10^{-5}	5.0×10^{-5}
ω (Cl^-)	[d^{-1}]	4.5×10^{-4}	4.5×10^{-4}	5.0×10^{-4}

References

Amos, R.T., Blowes, D.W., Bailey, B.L., Sego, D.C., Smith, L., and Ritchie, A.I.M. (2014). Waste-rock hydrogeology and geochemistry. Appl. Geochem.

Andrews, J.E., Brimblecombe, P., Jickells, T.D., Liss, P.S., and Reid, B. (2013). An Introduction to Environmental Chemistry (John Wiley & Sons).

Aziz, C.E., and Hatzinger, P.B. (2008). Perchlorate Sources, Source Identification And Analytical Methods. In In Situ Bioremediation of Perchlorate in Groundwater, H.F. Stroo, and C.H. Ward, eds. (Springer New York), pp. 55–78.

Bailey, B.L., Smith, L.J.D., Blowes, D.W., Ptacek, C.J., Smith, L., and Sego, D.C. (2013). Diavik Waste Rock Project: Persistence of contaminants from blasting agents in waste rock effluent. Appl. Geochem.

Bay, D.S., Peterson, H.E., Singurindy, O., Aranda, C.A., Dockrey, J.W., Sifuentes Vargas, F., Mayer, K.U., Smith, J.L., Klein, B., and Beckie, R. (2009). Assessment of neutral pH drainage from three experimental waste-rock piles at the Antamina mine, Peru. In Securing the Future and 8th International Conference on Acid Rock Drainage, (Skellefteå, Sweden), p. 11.

Blackmore, S. (2015). The role of hydrology, geochemistry and microbiology in flow and solute transport through highly heterogeneous, unsaturated waste rock at various test scales. PhD. University of British Columbia, Earth and Ocean Sciences.

Blackmore, S., Smith, L., Ulrich Mayer, K., and Beckie, R.D. (2014). Comparison of unsaturated flow and solute transport through waste rock at two experimental scales using temporal moments and numerical modeling. J. Contam. Hydrol. *171*, 49–65.

Chlot, S., Widerlund, A., and Öhlander, B. (2015). Nitrogen uptake and cycling in Phragmites australis in a lake-receiving nutrient-rich mine water: a 15N tracer study. Environ. Earth Sci. *74*, 6027–6038.

Corazao-Gallegos, C. (2007). The design, construction, instrumentation and initial response of a field-scale waste rock test pile.

Cvetkovic, V., Fiori, A., and Dagan, G. (2016). Tracer travel and residence time distributions in highly heterogeneous aquifers: Coupled effect of flow variability and mass transfer. J. Hydrol. *543, Part A*, 101–108.

Degnan, J.R., Böhlke, J.K., Pelham, K., Langlais, D.M., and Walsh, G.J. (2016). Identification of Groundwater Nitrate Contamination from Explosives Used in Road Construction: Isotopic, Chemical, and Hydrologic Evidence. Environ. Sci. Technol. *50*, 593–603.

Domenico, P., and Schwartz, F.W. (1990). Physical and chemical hydrogeology (John Wiley & Sons, Inc).

Eriksson, N., and Destouni, G. (1997). Combined effects of dissolution kinetics, secondary mineral precipitation, and preferential flow on copper leaching from mining waste rock. Water Resour. Res. *33*, 471–483.

Eriksson, N., Gupta, A., and Destouni, G. (1997). Comparative analysis of laboratory and field tracer tests for investigating preferential flow and transport in mining waste rock. J. Hydrol. *194*, 143–163.

Flury, M., and Papritz, A. (1993). Bromide in the Natural Environment: Occurrence and Toxicity. J. Environ. Qual. *22*, 747.

van Genuchten, M.T., and Wierenga, P.J. (1976). Mass Transfer Studies in Sorbing Porous Media I. Analytical Solutions. Soil Sci. Soc. Am. J. *40*, 473.

Haggerty, R., and Gorelick, S. (1995). Multiple-rate mass transfer for modeling diffusion and surface reactions in media with pore-scale heterogeneity. Water Resour Res *31*, 2383–2400.

Haggerty, R., and Reeves, P.C. (2002). STAMMT-L 1.0, Formulation and User's Guide, Technical Report ERMS 520308 (Sandia National Laboratories, Albuquerque, NM, USA).

Harvey, C., and Gorelick, S.M. (2000). Rate-limited mass transfer or macrodispersion: Which dominates plume evolution at the macrodispersion experiment (MADE) site? Water Resour. Res. *36*, 637–650.

Jermakka, J., Wendling, L., Sohlberg, E., Heinonen, H., and Vikman, M. (2014). Potential Technologies for the Removal and Recovery of Nitrogen Compounds From Mine and Quarry Waters in Subarctic Conditions. Crit. Rev. Environ. Sci. Technol.

Jodeiri Shokri, B., Doulati Ardejani, F., Ramazi, H., and Moradzadeh, A. (2016). Predicting pyrite oxidation and multi-component reactive transport processes from an abandoned coal waste pile by comparing 2D numerical modeling and 3D geo-electrical inversion. Int. J. Coal Geol. *164*, 13–24.

Karlsson, T., and Kauppila, T. (2016). Explosives-originated nitrogen emissions from dimension stone quarrying in Varpaisjärvi, Finland. Environ. Earth Sci. *75*, 1–8.

Lahmira, B., Lefebvre, R., Aubertin, M., and Bussière, B. (2016). Effect of heterogeneity and anisotropy related to the construction method on transfer processes in waste rock piles. J. Contam. Hydrol. *184*, 35–49.

Lahmira, B., Lefebvre, R., Aubertin, M., and Bussière, B. (2017). Effect of material variability and compacted layers on transfer processes in heterogeneous waste rock piles. J. Contam. Hydrol. *204*, 66–78.

Lefebvre, R., Hockley, D., Smolensky, J., and Lamontagne, A. (2001). Multiphase transfer processes in waste rock piles producing acid mine drainage: 2. Applications of numerical simulation. J. Contam. Hydrol. *52*, 165–186.

Liang, C.-P., Hsu, S.-Y., and Chen, J.-S. (2016). An analytical model for solute transport in an infiltration tracer test in soil with a shallow groundwater table. J. Hydrol. *540*, 129–141.

Lorca, M.E., Mayer, K.U., Pedretti, D., Smith, L., and Beckie, R.D. (2016). Spatial and Temporal Fluctuations of Pore-Gas Composition in Sulfidic Mine Waste Rock. Vadose Zone J. *15*.

Mahmood, F.N., Barbour, S.L., Kennedy, C., and Hendry, M.J. (2017). Nitrate release from waste rock dumps in the Elk Valley, British Columbia, Canada. Sci. Total Environ. *605*, 915–928.

Malmström, M.E., Destouni, G., and Martinet, P. (2004). Modeling Expected Solute Concentration in Randomly Heterogeneous Flow Systems with Multicomponent Reactions. Environ. Sci. Technol. *38*, 2673–2679.

Marcoline, J.R. (2008). Investigations of water and tracer movement in covered and uncovered unsaturated waste rock. PhD. University of British Columbia.

Molinari, A., Pedretti, D., and Fallico, C. (2015). Analysis of convergent flow tracer tests in a heterogeneous sandy box with connected gravel channels. Water Resour. Res. *51*, 5640--5657.

Neuner, M., Smith, L., Blowes, D.W., Sego, D.C., Smith, L.J.D., Fretz, N., and Gupton, M. (2013). The Diavik waste rock project: Water flow through mine waste rock in a permafrost terrain. Appl. Geochem. *36*, 222–233.

Nichol, C., Smith, L., and Beckie, R. (2005). Field-scale experiments of unsaturated flow and solute transport in a heterogeneous porous medium. Water Resour. Res. *41*, W05018.

Pedretti, D., and Bianchi, M. (2018). Reproducing tailing in breakthrough curves: Are statistical models equally representative and predictive? Adv. Water Resour. *113*, 236–248.

Pedretti, D., and Fernàndez-Garcia, D. (2013). An automatic locally-adaptive method to estimate heavily-tailed breakthrough curves from particle distributions. Adv. Water Resour. *59*, 52–65.

Pedretti, D., Lassin, A., and Beckie, R.D. (2015). Analysis of the potential impact of capillarity on long-term geochemical processes in sulphidic waste-rock dumps. Appl. Geochem. *62*, 75–83.

Pedretti, D., Molinari, A., Fallico, C., and Guzzi, S. (2016). Implications of the change in confinement status of a heterogeneous aquifer for scale-dependent dispersion and mass-transfer processes. J. Contam. Hydrol. *193*, 86–95.

Pedretti, D., Mayer, K.U., and Beckie, R.D. (2017). Stochastic multicomponent reactive transport analysis of low quality drainage release from waste rock piles: Controls of the spatial distribution of acid generating and neutralizing minerals. J. Contam. Hydrol. *201*, 30–38.

Peterson, H.E. (2014). Unsaturated hydrology, evaporation, and geochemistry of neutral and acid rock drainage in highly heterogeneous mine waste rock at the Antamina Mine, Peru.

Prasad, B., and Kumar, H. (2015). Treatment of Acid Mine Drainage Using a Fly Ash Zeolite Column. Mine Water Environ. 1–5.

Ramírez-Pérez, A.M., Paradelo, M., Nóvoa-Muñoz, J.C., Arias-Estévez, M., Fernández-Sanjurjo, M.J., Álvarez-Rodríguez, E., and Núñez-Delgado, A. (2013). Heavy metal retention in copper mine soil treated with mussel shells: Batch and column experiments. J. Hazard. Mater. *248–249*, 122–130.

Revey, G.F. (1996). Practical methods to control explosives losses and reduce ammonia and nitrate levels in mine water. Min. Eng. 61–64.

Salamon, P., Fernàndez-Garcia, D., and Gomez-Hernandez, J. (2007). Modeling tracer transport at the MADE site: The importance of heterogeneity. Water Resour. Res. *43*, W08404.

Shipitalo, M.J., and Edwards, W.M. (1996). Effects of initial water content on macropore/matrix flow and transport of surface-applied chemicals. J. Environ. Qual. *25*, 662–670.

Silva, N.C., Chagas, E.G.L., Abreu, C.B., Dias, D.C.S., Lopez, D., Guerreiro, E.T.Z., Alberti, H.L.C., Braz, M.L., Branco, O., and Fleming, P. (2014). Radon as a Natural Tracer for Gas Transport Within Uranium Waste Rock Piles. Radiat. Prot. Dosimetry ncu098.

Simunek, J., Jarvis, N.J., van Genuchten, M.T., and Gärdenäs, A. (2003). Review and comparison of models for describing non-equilibrium and preferential flow and transport in the vadose zone. J. Hydrol. *272*, 14–35.

Simunek, J.M., Van Genuchten, M.T., and Sejna, M. (2005). The HYDRUS-1D software package for simulating the one-dimensional movement of water, heat, and multiple solutes in variably-saturated media. University of California-Riverside Research Reports 3 (pp.1-240).

Smith, J.L., and Beckie, R.D. (2003). Hydrologic and geochemical transport processes in mine waste rock. In Environmental Aspects of Mine Wastes, J.L. Jambor, D.W. Blowes, and A.I.M. Ritchie, eds. (Ottawa: Mineralogical Association of Canada), pp. 51–72.

Speidel, B. (2011). Estimation of soil water characteristic curves in mine waste rock. Unpublished undergraduate thesis. The University of British Columbia.

Strömberg, B., and Banwart, S. (1999). Weathering kinetics of waste rock from the Aitik copper mine, Sweden: scale dependent rate factors and pH controls in large column experiments. J. Contam. Hydrol. *39*, 59–89.

Wilson, A.M., Woodward, G.L., and Savidge, W.B. (2016). Using heat as a tracer to estimate the depth of rapid porewater advection below the sediment–water interface. J. Hydrol. *538*, 743–753.

Xie, Y., Cook, P.G., Shanafield, M., Simmons, C.T., and Zheng, C. (2016). Uncertainty of natural tracer methods for quantifying river–aquifer interaction in a large river. J. Hydrol. *535*, 135–147.

Zaramella, M., Marion, A., Lewandowski, J., and Nützmann, G. (2016). Assessment of transient storage exchange and advection–dispersion mechanisms from concentration signatures along breakthrough curves. J. Hydrol. *538*, 794–801.

Zheng, C., Bianchi, M., and Gorelick, S.M. (2011). Lessons Learned from 25 Years of Research at the MADE Site. Ground Water *49*, 649–662.

Zinn, B., and Harvey, C.F. (2003). When good statistical models of aquifer heterogeneity go bad: A comparison of flow, dispersion and mass transfer in connected and multivariate Gaussian hydraulic conductivity fields. Water Resour. Res. *39*, 1051.